The Role of Insulating Oxides in Blocking the Charge Carrier Recombination in Dye-Sensitized Solar Cells

Aravind Kumar Chandiran, Mohammad K. Nazeeruddin, and Michael Grätzel**

Electron recombination is one of the major loss factors in dye-sensitized solar cells (DSC), especially, with single electron outer sphere redox shuttle electrolyte. Insulating sub-nanometer oxide tunneling layers deposited by atomic layer deposition (ALD) are known to block the electron recombination, thereby leading to an increase in the open-circuit potential and the collection efficiency of the solar cell. A general perception in the DSC community is that any insulating oxide layer can block the recombination. However, in this work, it is unraveled that the insulating property of oxides alone is not sufficient. In addition, the properties such as the conduction band position and the oxidation state of the insulating oxide, the electronic structural modification induced to the underlying TiO_2 mesoporous film, modification of surface charges (isoelectric point) and charge of the electrolyte species have to be considered. A complete photovoltaic study is done by depositing different cycles (by ALD) of four different insulating oxides (Ga_2O_3, ZrO_2, Nb_2O_5, and Ta_2O_5) and their recombination characteristics, surface electronic properties, transport rate, and injection dynamics are investigated with a standard organic dye and Co^{2+}/Co^{3+} redox mediator. A comparison is made with the conventional iodide/triiodide electrolyte.

1. Introduction

Recently, dye-sensitized solar cells (DSC) have attracted enormous research and commercial interest due to their potential to economically convert the solar light to electricity.[1–3] A typical DSC is a sandwich of a photoactive dye sensitized mesoporous TiO_2 film and a catalyst coated counter electrode, with a redox electrolyte between them. The illumination of the device results in the optical excitation of dye molecules and the excited electrons are injected into TiO_2 on the fs–ps time scale, due to sufficient electronic overlap of lowest unoccupied molecular orbitals (E_{LUMO}) of the dye and the conduction band of titanium dioxide (E_{CB}). This injection process is followed by the regeneration of oxidized sensitizer by the donation of electrons from the reduced redox component in the electrolyte. Finally, the whole cycle of the device function completes by the transfer of the photogenerated electrons in the TiO_2 to the counter electrode via the external circuit regenerating the electrolyte.[4–6] Lately, attention has shifted from the classical Ru(II) polypyridyl sensitizer and I^-/I_3^- redox shuttle, respectively, to Zn (II) porphyrins or organic sensitizer and Co^{2+}/Co^{3+} electrolyte due to their competence in demonstrating high photovoltaic power conversion efficiency (PCE) approaching 13%.[7,8] The intrinsic advantage of Co^{2+}/Co^{3+} redox shuttle is that it consumes less driving force ($E_{Red/Ox}$–$E_{HOMO:Dye}$), as low as ≈200 mV, to regenerate the oxidized dye sensitizer compared to ≈500 mV regeneration loss for I^-/I_3^- electrolyte. This increases the open-circuit potential (V_{OC}) in the former case and hence the attainable, power conversion efficiency (PCE). However, the advantages of Co^{2+}/Co^{3+}, in the terms of regeneration, come at the expense of fast recombination kinetics of the photogenerated electrons in the TiO_2 to Co^{3+} by the outer-sphere redox mechanism. At open-circuit, the high recombination rate reduces the steady state electron density in the conduction band of TiO_2 ($_{Ti}E_{CB}$) and in turn, it lowers the quasi-Fermi level resulting in the low V_{OC}. At short-circuit the same process can decrease the fill factor (FF) and the collection efficiency of the device.[5,9,10] In order to utilize effectively the outer sphere redox mediators, like Co^{2+}/Co^{3+}, Fc/Fc^+, an efficient oxide blocking layer on the surface of TiO_2 is warranted to suppress the back reaction kinetics.[11–16] So far in the DSC community, two fundamental criteria were considered for the selection of an effective blocking layer: The layer has to be 1) insulating and 2) ultrathin to allow the efficient injection of electrons from the excited state of the dye into the TiO_2 and at the same time the recombination kinetics has to be delayed, in short, a tunneling layer is necessary. Several insulating layers such as Ga_2O_3, Al_2O_3, ZrO_2, SiO_2, HfO_2, and MgO have been investigated as blocking layers and also in some cases, to enhance the stability of adsorbed dye molecules.[11–15,17–23] Conventional oxide deposition techniques like sol–gel, chemical vapor deposition, or physical vapor deposition can lead to uneven and thicker oxide layers or are ineffective in making a deposition on high aspect ratio structures. So in order to achieve a conformal, pinhole-free and ultrathin deposition on any arbitrary mesoporous films, the atomic layer deposition (ALD) technique was successfully employed. The growth

A. K. Chandiran, Dr. M. K. Nazeeruddin, Prof. M. Grätzel
Laboratory of Photonics and Interfaces
Institute of Chemical Sciences and Engineering
Swiss Federal Institute of Technology (EPFL)
Station 6, 1015, Lausanne, Switzerland
E-mail: mdkhaja.nazeeruddin@epfl.ch;
michael.graetzel@epfl.ch

DOI: 10.1002/adfm.201302352

proceeds by introducing a reactive metal precursor (X-M-X) which, for instance, reacts with hydroxyl groups on the substrate's surface (S-OH) to form S-O-M-X layer and the excess precursors (X-M-X) and reaction by-products (XH) are purged out using an inert gas carrier. In the second step, an oxidizing precursor (H_2O) is pulsed in to the reactor which regenerates the hydroxyl groups (S-O-M-OH) for the subsequent deposition. Each metal precursor pulse-inert gas purge-oxidized precursor pulse-inert gas purge contributes to one cycle of deposition. As the metal and oxidizing precursors are pulsed at two different stages and because the precursors pulsed into the reactor are in gaseous phases, deposition of conformal layers on the high aspect ratio structures become possible.[24–26] The aforementioned property is highly needed in DSC, as the photoanode used is a mesoporous TiO_2 with complicated pore morphology. On this road, we previously employed insulating sub-nanometer gallium oxide to block the back reaction efficiently and it lead to a record V_{OC} of 1.12 V.[11] The general perception in the DSC community is that any insulating layers can block the back reaction. However, further scrutiny revealed that just the insulating property is not sufficient to block the back reaction. We found that the properties such as conduction band position and the oxidation state of the insulating oxide, the electronic structural modification induced to the underlying TiO_2 mesoporous film, modification of surface charges (isoelectric point) and charge of the electrolyte species have to be considered. To get a clear and generalized perception in terms of blocking layer, we selected four different insulating oxides, two of them with the bulk conduction band position higher (gallium oxide $_{Ga}E_{CB}$ = –2.95 eV/vacuum, zirconium oxide $_{Zr}E_{CB}$ = –3.4 eV/vacuum) and two lower (niobium oxide $_{Nb}E_{CB}$ = –4.33 eV/vacuum, tantalum oxide $_{Ta}E_{CB}$ = –4.59 eV/vacuum) than both the conduction band of TiO_2 ($_{Ti}E_{CB}$ = –4.0 eV/vacuum) and the LUMO of our standard organic dye sensitizer ($_{Y123}E_{LUMO}$ = –3.5 eV/vacuum).[27,28] The photovoltaic properties and electron transfer dynamics were investigated in detail with our standard Co^{2+}/Co^{3+} and also with I^-/I_3^- electrolyte.

2. Results and Discussion

The photoanode used in the study consists of 5 nm ALD underlayer TiO_2 on a precleaned transparent conducting oxide glass. Our previous study have shown that a pinhole free 5 nm ALD TiO_2 is sufficient to block the back reaction from TCO glass by inhibiting the intimate contact with Co^{2+}/Co^{3+} redox electrolyte.[11,29] Then a 3 µm TiO_2 (particle size: 20 nm, pore diameter: 32 nm) is screen printed and the films were sintered by a series of firing steps up to 500 °C to remove polymeric binders and to ensure better electronic contact between nanoparticles. The combination of 3 µm TiO_2 film with 32 nm pore diameter was selected to ensure uniform diffusion of the ALD metal oxide precursors throughout the film. The complete experimental procedure of ALD, material and photovoltaic characterizations are given in the experimental section.

2.1. Material Characterization

Different cycles of Ga_2O_3, ZrO_2, Nb_2O_5, and Ta_2O_5 were then deposited on the mesoporous film by atomic layer deposition at relatively low temperatures of 150 °C expect for Ta_2O_5 (200 °C).[30–33] Similar depositions were carried out on a Si wafer and their growth rate (nm per cycle of deposition) was estimated using spectroscopic ellipsometry. The growth rates for Ga_2O_3, ZrO_2, Nb_2O_5 and Ta_2O_5 were found to be 0.1, 0.13, 0.05, and 0.13 nm per cycle, respectively. Like in our previous studies, we stress a point that the first few cycles of deposition on the mesoporous TiO_2 may be different from the actual growth rate measured on the Si wafer (with native oxide) due to the difference in the surface acid-base properties of the depositing substrate.[11,29,34] Following the thickness analysis, the mesoporous TiO_2 films with and without oxide ALD layers (5 cycles) were studied by X-ray photoelectron spectroscopy (XPS). All the binding energy (BE) values given below are calibrated with respect to the C 1s peak at 284.6 eV. The reference TiO_2 exhibits Ti $2p_{3/2}$ and Ti $2p_{1/2}$ core electron BE peaks at 458.65 eV and 464.34 eV, respectively confirming the presence of Ti in 4+ oxidation state.[35] The elemental Ga, Zr, Nb, and Ta from their corresponding oxide overlayers show binding energy peaks at 1117.96 eV (Ga $2p_{3/2}$), 182.44 eV (Zr $3d_{5/2}$), 184.81 eV (Zr $3d_{3/2}$), 206.94 eV (Nb $3d_{5/2}$), 209.71 eV (Nb $3d_{3/2}$), and 25.9 eV (Ta $4f_{7/2}$). These peaks evidence the presence of Ga, Zr, Nb and Ta in +3, +4, +5, and +5 oxidation states, respectively.[36–39] In the case of films containing insulating ALD oxide layers, the Ti ion is mostly present in 4+ oxidation states but the Ti 2p core BE peaks are shifted to lower values possibly due to the presence of high concentration of defects. The deposition of oxides of Ga and Zr, shifts the BE of Ti $2p_{3/2}$ to the lower side by 0.1–0.2 eV whereas Nb and Ta oxides shift by 0.4 eV. The significant shift in the latter case also indicates the formation of Ti^{3+} in order to balance the excess charge carriers of 5+ cation.[40] All the XPS plots are displayed in Figure S1–S6. As the deposited layers are less than 1 nm, we expect them to be amorphous on the surface of the mesoporous titanium dioxide film.

2.2. Photovoltaic Characterization–Evolution of V_{OC}

The dye-sensitized solar cells are made with the reference bare TiO_2 and the modified photoanodes with different oxide insulating layers with our standard D-π-A organic dye sensitizer (Y123, Figure S7A, Supporting Information) and cobalt(bipyridine-pyrazole)$_2^{2+/3+}$ redox mediator (Figure S7B, Supporting Information). The devices are constructed following the procedure similar to the conventional DSC, except that before dipping, the photoanodes were treated in O_2 plasma for 5 min instead of heat treatment at 500 °C. The thermal treatment will increase the energy of atoms allowing the surface cations (Ga^{3+}, Zr^{4+}, Nb^{5+}, or Ta^{5+}) in the ALD layer to diffuse inside the TiO_2 lattice. These diffused atoms can act as dopants or cationic substituents rather than as a tunneling layer.[41]

The DSC with the reference TiO_2 exhibits an open-circuit potential (V_{OC}) of 1016 mV. The deposition of gallium oxides up to 2 cycles did not change the V_{OC} but beyond 3 cycles, V_{OC} increased significantly by around 60 mV. Similar to the Ga_2O_3, the deposition of ZrO_2 also enhanced the V_{OC} to ≈1070 mV. However, the deposition of Nb_2O_5 and Ta_2O_5 significantly lowered the V_{OC} even at the very first few cycles. With 6 cycles of Nb_2O_5, the V_{OC} declined to 877 mV, which is ≈140 mV less

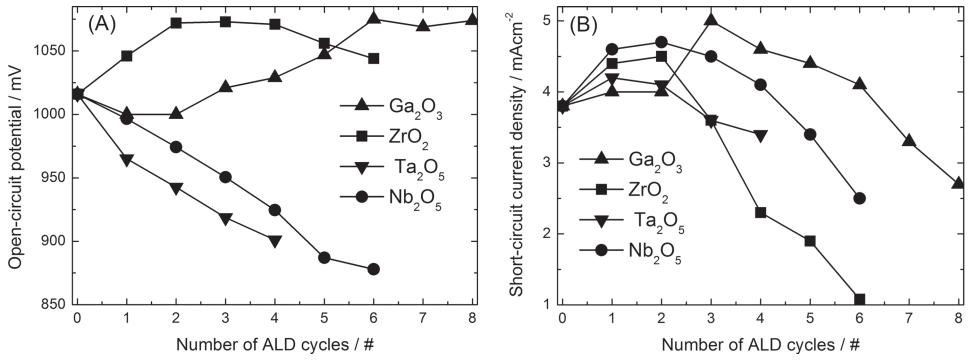

Figure 1. Evolution of A) open-circuit potential and B) short-circuit current density for dye-sensitized solar cells made with different cycles of ALD oxide overlayers on the mesoporous TiO_2. (Ga_2O_3–up triangle; ZrO_2–square; Ta_2O_5–down triangle; Nb_2O_5–circle).

than the reference device. Similarly, with 4 cycles of Ta_2O_5, the V_{OC} is reduced to ≈900 mV. The plot of variation of V_{OC} as a function of the number of ALD cycles for different overlayers is displayed in **Figure 1**A.

In a typical dye-sensitized solar cell, the open-circuit potential is primarily dependent on three factors: 1) the distribution of trap states or the conduction band shift, 2) recombination rate of photogenerated electrons from TiO_2 to the redox mediators, and 3) the Nernst potential of the redox electrolyte.[5,10] As the redox mediators used in this study is similar, no change in V_{OC} is expected and the third parameter is excluded from the discussion. The first two parameters are analyzed separately to find the origin of the variation in V_{OC}.

2.2.1. Trap States Distribution

The trap states distribution of the TiO_2 film in the DSC is measured using the charge extraction technique and is displayed in **Figure 2**.[42] The reference TiO_2 film exhibits an exponential dependence of the trap states distribution with increasing voltage (hollow squares, Figure 2), that is, when moving towards the conduction band. The deposition of ZrO_2 and Ga_2O_3 on the titanium dioxide mesoporous film did not significantly affect the surface trap states and the distribution overlaps with the reference TiO_2 (column 1,2 in Figure 2).[11] The pentavalent oxide ALD layers on the surface of titania, however, significantly enhanced the electronic defects. One cycle of Nb_2O_5 slightly shifted down the trap states distribution and further increase in the deposition cycles, brought down the trap states by around 120 mV (at higher charge densities). Similarly, tantalum oxide increased the mid-gap defect states right from the first cycle of deposition. There are two possibilities for the observed modification in the trap states with the pentavalent oxides: 1) formation of Ti^3+ or titanium vacancies and/or 2) hybridization of Nb 4d and Ta 5d electronic levels with the surface Ti 3d orbitals to create shallow donor electronic levels

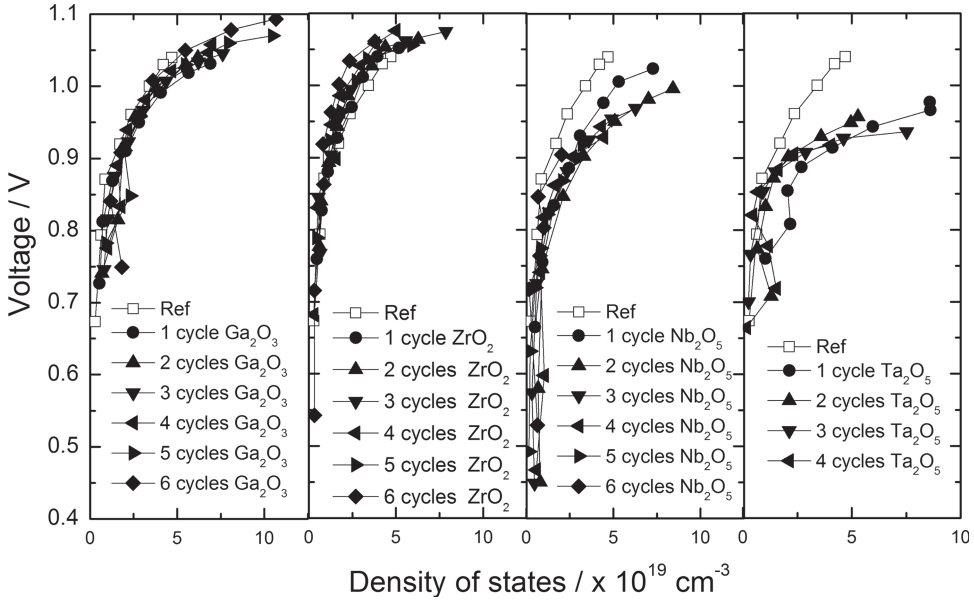

Figure 2. The distribution of the electronic trap states in the forbidden optical band gap for the reference TiO_2 film (hollow squares) and with different ALD oxide overlayers. (column 1–Ga_2O_3; column 2–ZrO_2; column 3–Nb_2O_5; column 4–Ta_2O_5).

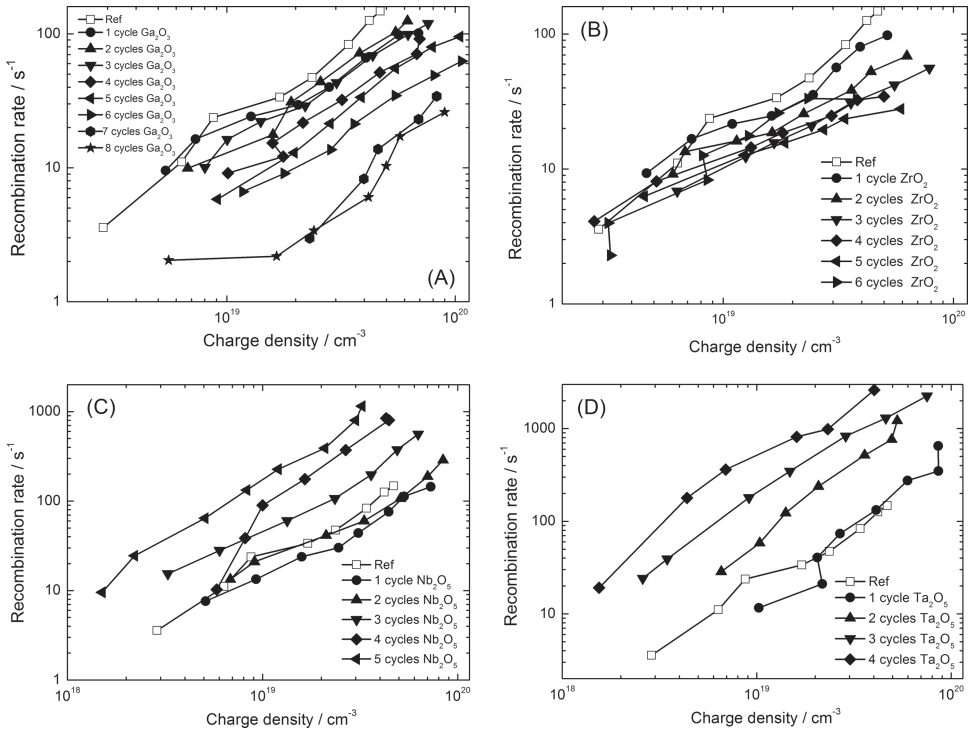

Figure 3. The recombination rate of photogenerated electrons in the reference TiO_2 device (solid hollow squares) to Co^{3+} redox mediator is compared with devices containing different insulating oxide ALD overlayers such as A) Ga_2O_3, B) ZrO_2, C) Nb_2O_5, and D) Ta_2O_5.

below the conduction band of TiO_2.[43–46] As discussed before in XPS section, there is an evidence for the presence of Ti^{3+}. Previously, we have shown that the bulk doping of Nb increases the defect states below the conduction band shown to originate both from the Ti^{3+}/oxygen vacancies and shallow donor levels of Nb 4d orbitals.[47] Likewise, the present case of surface tunneling overlayer can also be visualized partly as a surface doping of TiO_2. The first ALD monolayer on the surface can involve in the hybridization with the parent metal oxide lattice leading to the formation of donor levels or electron traps. So, for a given photogenerated charge density in the TiO_2, the increase in the trap states with the pentavalent oxide surface modification, decrease the quasi Fermi level of electrons lowering the V_{OC}.[6,10]

2.2.2. Electron Recombination

The recombination rate of the electrons in the TiO_2 is measured by transient photovoltage decay technique and is plotted as a function of charge density in **Figure 3**. The deposition of Ga_2O_3 and ZrO_2 decreases the recombination rate with the number of ALD cycles. However the deposition of pentavalent oxides significantly increased the recombination. Just with 4–5 cycles, the rate of electron back reaction is increased by an order of magnitude. For a given charge density and a given trap states distribution, the film with low recombination kinetics maintains higher steady-state electron density and hence the quasi-Fermi level of electrons in the TiO_2 film is moved toward the conduction band, leading to an increase in the V_{OC}. The case is reverse when the recombination is higher.

The following discussion explains why there should exist a significant variation in the recombination properties with different sub-nanometer oxide overlayers. First let us start the discussion in terms of the occupation of the trap levels (Figure 2) across the nanoparticles in the case of niobium and tantalum oxide modified photoanodes. By bulk doping, like in reference,[47] the shallow donor levels (Nb 4d orbitals) below the conduction band of titanium dioxide exists across the cross-section of any given nanoparticle (assuming uniform distribution of dopants) and the distribution of defect states in the forbidden optical band gap can be considered to be the uniform. But, in the present case, the ALD oxides are deposited only as an overlayer on the TiO_2 and hence the donor levels are expected to be present only on the surface. So the density of the defect states is higher at the surface than at the bulk which leads to a creation of an electrical diffusion potential. This can induce a back flow of electrons from the bulk of TiO_2 to the surface, leading to an increase in the recombination. Secondly, we observed an unexpected trend in the transport rate (**Figure 4** and Figure S8, Supporting Information) of photogenerated electrons in photoanode films containing different oxide ALD layers. With Nb_2O_5 and Ta_2O_5 ALD overlayers, the transport rate is increased significantly compared to the reference TiO_2 device, despite the fact that overlayers increased the trap states distribution. It has to be noted that the deeper trap states are known to decrease the mobility of electrons in the film due to the increase in the trapping-detrapping time.[6] On other hand, the deposition of gallium oxide declined the rate of electron transport, whereas the zirconium oxide did not change the parameter significantly. This variation can be visualized again in terms of surface

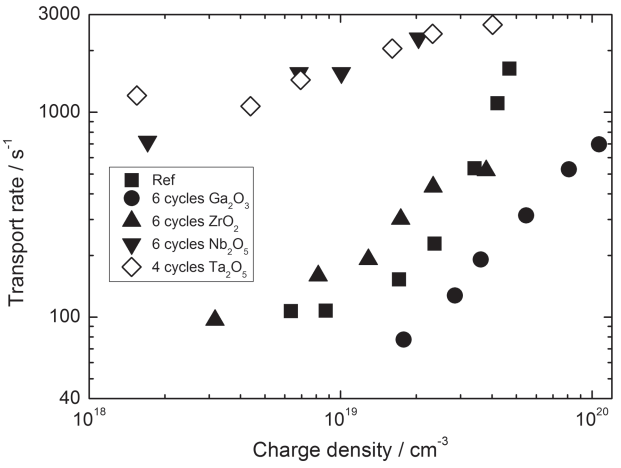

Figure 4. The transport rate of photogenerated electrons at short-circuit with and without ALD insulating oxide overlayers on the TiO_2 mesoporous film is plotted as a function of charge density.

doping of TiO_2 by the overlayers. The interface n-doping by Nb^{5+} and Ta^{5+} can increase the free electron density in the TiO_2 film leading to an increase in the conductivity. This in turn will increase the reactivity of the Co^{3+} towards the TiO_2, accelerating the recombination loss. Additionally, one has to note that both the Nb and Ta oxides possess low isoelectric point (pI– ≈ 2) compared to TiO_2 (pI– ≈ 5–8).[27] So when the electrolyte of pH higher than the surface pI comes in contact with the photoanode, the surface becomes more negatively charged and it can attract positively charged cobalt complex leading to the increase in the recombination rate. There is an indirect evidence to support the modification in the surface charges which is discussed in the later part of this manuscript. So the primary effect of back reaction with the niobium and tantalum oxide ALD layers comes from cumulative effect of intrinsic electric field across the nanoparticle, increased film conductivity and negative surface charge.

The Ga^{3+} which is one electron deficient compared to the Ti^{4+} can compensate for the existing oxygen vacancy in TiO_2 decreasing the conductivity of the film. This observation is consistent with our bulk doping of TiO_2 by Ga.[48] So, the blocking effect of Ga_2O_3 tunnelling layers comes from the cumulative effect of decreased TiO_2 film conductivity and increased distance between the electrolyte component and the electrons in TiO_2 due the presence of ALD layer leading to an exponential decrease in recombination rate, according to Marcus theory.

Furthermore, the dummy cells without dyes were made to exclude the effect of the dye packing and the recombination properties were analyzed using electrochemical impedance spectroscopy (Figure S9, Supporting Information). A trend of low recombination rate with Ga_2O_3 and ZrO_2 and high recombination rate with Nb_2O_5 and Ta_2O_5 ALD overlayers is observed compared to the reference TiO_2 dummy device. The impedance spectroscopic result is supported by the cyclic voltammetric data in Figure S10 (Supporting Information). For more details on EIS and CV, please see the supporting information. The results observed EIS and CV are consistent with the recombination rate measurements by transient photovoltage decay.[49]

2.3. Photovoltaic Characterization–Evolution of J_{SC}

Following the detailed study of the variation in the open-circuit potential of the device in the preceding section, the dependence of the short-circuit current density with different oxide ALD overlayers is explored. Figure 1B shows the plot of J_{SC} as a function of number of ALD cycles. The reference device generated a current density of 3.8 mA/cm^2 and with the deposition of first few cycles of insulating ALD layers, current density has increased followed by a drop. The deposition of 3 cycles of Ga_2O_3 increases the current density to a maximum of 5 mA/cm^2.

To investigate the variation in the current density, the dye uptake (Figure S11, Supporting Information) and the injection dynamics (**Figure 5**) were studied. The deposition of Ga_2O_3 slightly reduced the dye uptake compared to the reference TiO_2 film and is followed by the ZrO_2. The pentavalent oxides decreased the dye loading on the surface significantly. A decrease of 1/3 and 1/2 concentration of dye with respect to the reference film are observed for the Ta_2O_5 and Nb_2O_5 modified samples, respectively. As mentioned before, these two oxides have very low isoelectric point making the surface more negatively charged. Hence the dye molecules which are also negatively charged are repelled from the surface of the photoanode film, thereby decreasing the dye uptake.

2.3.1. Excited State Electron Injection

To analyze the kinetics of photoexcited electron injection, we monitored the fluorescence decay of the Y123 dye sensitized films (Figure 5).[50] The excited state lifetimes of Y123 dye in the two extreme cases of completely injecting (reference TiO_2) and non-injecting samples (Al_2O_3) are compared with ALD overlayer modified TiO_2 films. The half-lifetime of excited electrons in the reference TiO_2 is 180 ps and 685 ps with Al_2O_3 films. The deposition of Ga_2O_3 increased the lifetime progressively through 315 ps, 330 ps, and 430 ps for 2, 4, and 6 cycles, respectively. Similarly, an increase in the lifetime is observed by the deposition of ZrO_2, but more steeply. With just two cycles of ZrO_2, the lifetime increased to 391 ps. As the lifetimes in the both the aforementioned cases are higher than the Y123 sensitized bare TiO_2 film, it is ascertained that the injection is blocked to a significant extent from the very first cycles of deposition and is being pushed toward completely non-injecting regime. In DSC, however, we have to note that the current-density of the corresponding surface modified films are higher than reference and the increase in J_{SC} could be attributed to the enhanced collection efficiency of the devices as described in our previous work.[11]

On other hand, the deposition of pentavalent oxides slightly reduced the lifetime of excited electrons compared to the reference. This indicates that the injection of electrons from the LUMO levels of the dye to the photoanode film is improved. This observation in conjunction with the enhanced transport rate (Figure 4) with the Nb_2O_5 and Ta_2O_5 surface treated films is responsible for the increase in the short-circuit current density

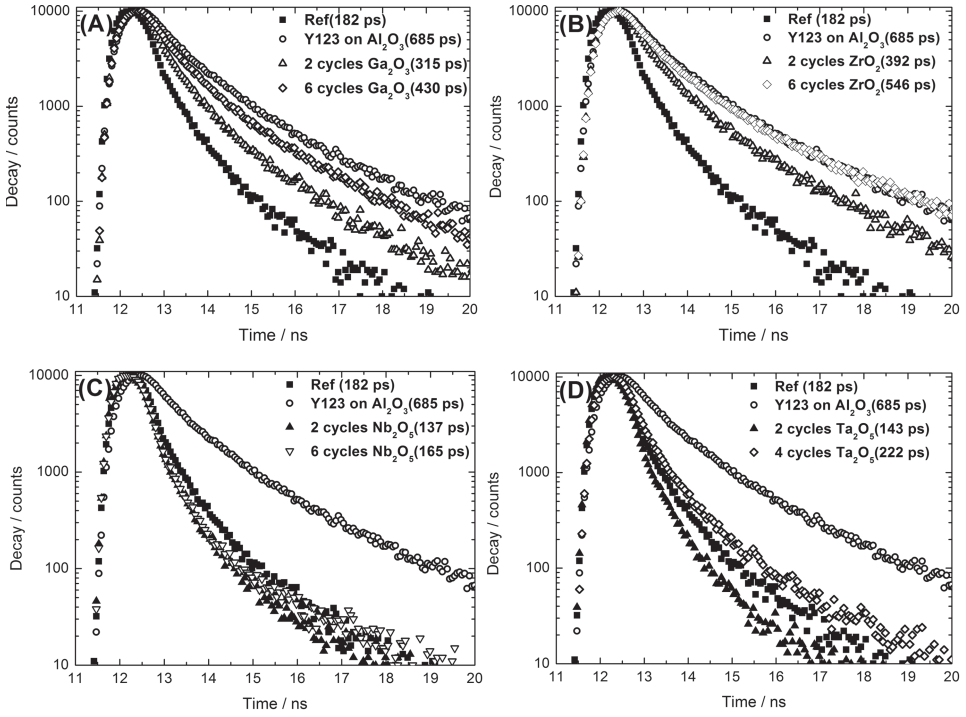

Figure 5. The fluorescence emission decay for Y123 sensitized reference TiO_2, non-injecting Al_2O_3 and ALD insulating oxide overlayers such as A) Ga_2O_3, B) ZrO_2, C) Nb_2O_5, and D) Ta_2O_5 on the surface of mesoporous TiO_2, measured by the time-resolved single photon counting (TRSPC). The numbers indicated in the brackets in the legends correspond to their respective lifetime.

during the first few cycles of deposition, despite an observation of the reduction in dye uptake and high recombination rate.

The evolution of other photovoltaic parameters such fill factor and the device power conversion efficiency are displayed in Figure S12–S13 (Supporting Information). All the corresponding *J–V* curves with different insulating oxides are given in Figure S14–S17.

2.4. Blocking Layer with Iodide/Triiodide Redox Mediator

To generalize to concept of ALD tunneling overlayers, we also have tested similar devices with our standard iodide/triiodide electrolyte. The bare TiO_2 film exhibits a J_{SC} and V_{OC} of 11.0 mA cm^{-2} and 776.9 mV respectively. The deposition of 5 cycles of Ga_2O_3 increased 50 mV in V_{OC} and lowered the current density to around 5.9 mA cm^{-2}. With Nb_2O_5, no change in the J_{SC} is observed but V_{OC} declined by around 50 mV (**Figure 6**A). The recombination rates of electrons for three aforementioned devices are given in the Figure 6B. Compared to the reference device the recombination rate is higher for the devices with Nb_2O_5 overlayer and lower for Ga_2O_3. The explanation for the trend observed in the recombination rate for Ga_2O_3 is same as described for Co^{2+}/Co^{3+} electrolyte. But for Nb_2O_5, the surface pI has to affect the recombination rate in opposite way for I^-/I_3^-. The negative charge of the surface due to the deposition of Nb_2O_5 has to repel the negative charged I_3^- away and it is expected to retard the recombination. However, the

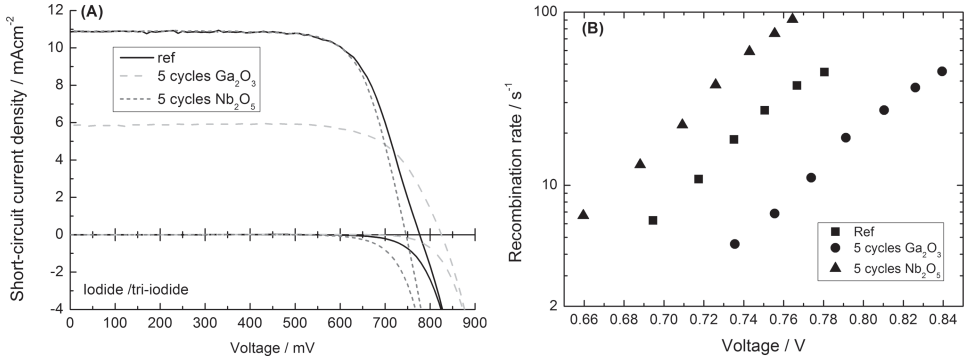

Figure 6. A) Current-voltage characteristics of iodide/triiodide based DSC with and without ALD insulating layers on the reference TiO_2, and their corresponding B) recombination plots measured by transient photovoltage decay.

Table 1. Carrier gas flow and deposition conditions of metal precursors in ALD.

Precursor	Precursor temperature [°C]	Pulse time [ms]	Reactor temperature [°C]	Carrier flow [sccm]
tris(dimethylamido)gallane dimer	130	100	150	10
tetrakis(dimethylamido)zirconium	75	100	150	10
(t-butylimido)tris(diethylamido)niobium	110	500	150	20
tantalum ethoxide	105	1000	200	5

deeper trap states distribution, the increase in the conductivity of the film and the surface electric field could be responsible for the decrease in the V_{OC}. The trend observed with the iodide/triiodide is consistent with the Co^{2+}/Co^{3+} redox electrolyte.

3. Conclusion

In this work, we have examined the effect of tunneling layers for dye-sensitized solar cells to block the interfacial charge carrier recombination reaction. Our investigation reveals that the insulating property of oxide alone is not sufficient to suppress this unwanted back reaction. In order to effectively implement a tunneling layer, the properties such as conduction band position and oxidation state of the ALD oxide have to be considered as primary criteria. The surface isoelectric property of the insulating layer also has to be considered with regards to the charge of the electrolyte redox species. Our work concludes that Ga_2O_3 or ZrO_2 can be a good tunneling layer to arrest the interfacial recombination of photogenerated carriers. The selection of pentavalent oxides introduces shallow donor levels below the conduction band of titanium dioxide. The ionized donors can act as traps for electrons reducing the attainable open-circuit potential. In addition, due to surface doping, the conductivity of the film is increased which in turn increases the loss of photogenerated electrons to Co^{3+}. An electric field that might exist between the trap states in bulk and on surface also affects the electron back reaction. Most of the previous studies on the tunneling layers compared single oxide layers whereas in this study, we made an exhaustive comparison of 4 different oxides with different thickness and two mostly used electrolyte species in liquid DSC. Further work has to aim at a clear understanding of the interface between the blocking layer and the TiO_2. This work can be considered as a model investigation that can be extended readily to other photoelectrochemical systems.

4. Experimental Section

Preparation of TiO_2 Photoanode Film: A 5 nm compact TiO_2 is deposited onto a precleaned transparent conducting glass (TEC15, Solaronix, Switzerland) by atomic layer deposition technique (Savannah S100, Cambridge Nanotech, USA). The deposition of ALD TiO_2 is carried out using tetrakis(dimethyl amido) titanium (TDMAT, 75 °C Aldrich, Germany) as a metal precursor and deionized H_2O (18 MΩ, 25 °C) as an oxidizing precursor. Following the 100 ms pulse of TDMAT or 10 ms pulse of H_2O, the precursors are confined inside the ALD reactor (120 °C) for 5 s (exposure time) to ensure a complete exposure of the surface of the photoanode. The excess precursors and the reaction by-products are purged out using a nitrogen carrier gas for 10 s. TDMAT pulse-purge-H_2O pulse-purge contributes to one cycle of deposition. 75 cycles of deposition were carried out to attain 5 nm of TiO_2 on the TCO glass.[11,25,26]

After the underlayer deposition, 2.7 ± 0.1 μm our standard titanium dioxide paste (20 nm particle size and 32 nm pore size) is screen printed. The films are then sintered following a series of firing steps (325 °C for 5 min with 15 min ramp time, 375 °C for 5 min with 5 min ramp time, 450 °C for 15 min with 5 min ramp time and 500 °C for 15 min with 5 min ramp time) to remove the polymeric binders and to ensure better electronic contact between particles.[41] The thicknesses of screen printed films were measured using a KLA Tensor Alpha-Step 500 profilometer.

Deposition of ALD Insulating Ga_2O_3, ZrO_2, Nb_2O_5, and Ta_2O_5: The metal precursors used in the study are tris(dimethylamido)gallane dimer, tetrakis(dimethylamido)zirconium, (t-butylimido)tris(diethylamido) niobium and tantalumethoxide for Ga_2O_3, ZrO_2, Nb_2O_5, and Ta_2O_5 deposition respectively. The oxidizing precursor used in the all cases is deionized H_2O (18 MΩ, 25 °C). The metal precursor is pulsed in to the reactor by ultradry N_2(99.99%) carrier gas and the precursor is confined into the reactor for 30 s (waiting time) to ensure complete diffusion inside the mesoporous TiO_2. Then the excess precursors and the reaction by-products are purged out for 30 s (purging time). This is followed by a pulsing of H_2O (15 ms pulsing time) with 30 s waiting time and 30 s purging time similar to the metal precursors. The complete details of the metal precursor temperature, metal precursor pulsing time, reactor temperature and the carrier flow are displayed in the **Table 1**.[30–33]

Material Characterization: For the identification of thickness of ALD layers, 100–200 cycles with identical growth conditions were deposited on Si wafers and measured using spectroscopic ellipsometer with photon energies over the range of 1 to 6 eV (Sopra GES 5E). The chemical properties of the deposited ALD layers on the mesoporous TiO_2 were probed using X-ray photoelectron spectrometer (XPS/ESCA KRATOS AXIS ULTRA) with Al K α X-ray radiation of 1486.7 eV.

Device Fabrication: The blank TiO_2 and ALD insulating layer passivated TiO_2 mesoporous photoanodes were cleaned using an oxygen plasma (Harrick plasma, USA) for 5 min to remove the surface contaminants and the films are sensitized in a 0.1 mM Y123 solution in 50/50 (v/v) acetonitrile/t-butanol mixture for 8 h. The sensitized electrodes were then washed in acetonitrile to remove the loosely bound dye molecules before the cell assembly. The counter electrode was made by drop casting carbon (ABCR, Germany) from an acetone solution on the FTO glass (TEC7, Solaronix, Switzerland). The two electrodes were melt sealed using a 25 μm thick surlyn™ (Dupont, USA) polymer film. The electrolyte used was a mixture of 200 mM Co^{2+}, 50 mM Co^{3+}, 100 mM $LiClO_4$, and 200 mM tert-butyl pyridine in acetonitrile solvent. This electrolyte was injected by vacuum back filling technique through a hole sand-blasted at the side of the counter electrodes. Finally the holes were sealed and contacts were made for testing. For dummy cells, similar fabrication procedure was followed expect the dye-sensitization.[41,47]

Photovoltaic Characterization: A 450W xenon lamp (Oriel, USA) was used as light source for photovoltaic (*J–V*) measurements. The spectral output of the lamp was filtered using a Schott K113 Tempax sunlight filter (Präzisions Glas & Optik GmbH, Germany) to reduce the mismatch between the simulated and actual solar spectrum to less than 2%. The *J–V* characteristics of the cells were recorded with a Keithley model 2400

digital source meter (Keithley, USA). The photo-active area of 0.159 cm^2 was defined using a blackened metal mask. The electron recombination and transport in the mesoporous film was measured by transient photovoltage and photocurrent decay measurements, respectively. The white light was generated by an array of LEDs while a pulsed red light (0.05 s square pulse width) was controlled by a fast solid-state switch to ascertain rapid sub-millisecond rise of light perturbation. The current and voltage decay were recorded on a mac-interfaced Keithley 2602 source meter.

Cyclic Voltammetry (CV) and Electrochemical Impedance Spectroscopy (EIS): CV and EIS measurements were obtained using an AUTOLAB potentiostat (PGSTAT 302N, Netherlands). Dummy cells without sensitizers were used for measurements where the anode was connected to the working electrode and the counter electrode to the reference and the cathode. The impedance response was measured over the frequency range of 100 kHz to 10 mHz at the applied forward bias of 0.9 V in dark.

Supporting Information

Supporting Information is available from the Wiley Online Library or from the author.

Acknowledgement

The authors acknowledge the financial contribution from EU FP7 project "ORION" (grant agreement number NMP-229036) and MOLESOL (the FP7-Energy-2010-FET project contract No. 256617). M.K.N. acknowledge the support from the World Class University program, Photovoltaic Materials, Department of Material Chemistry, Korea University, funded by the Ministry of Education, Science and Technology through the National Research Foundation of Korea (No. R31–2008–000–10035–0) for Adjunct Professor appointment. The authors are grateful for the financial support from the Balzan Foundation as a part of the 2009 Balzan prize awarded to M.G.

Received: July 12, 2013
Revised: September 4, 2013
Published online: October 14, 2013

[1] M. Gratzel, *Nature* **2001**, *414*, 338.
[2] B. O'Regan, M. Grätzel, *Nature* **1991**, *353*, 737.
[3] H. Pettersson, K. Nonomura, L. Kloo, A. Hagfeldt, *Energy Environ. Sci.* **2012**, *5*, 7376.
[4] A. Listorti, B. O'Regan, J. R. Durrant, *Chem. Mater.* **2011**, *23*, 3381.
[5] A. Hagfeldt, G. Boschloo, L. Sun, L. Kloo, H. Pettersson, *Chem. Rev.* **2010**, *110*, 6595.
[6] P. R. F. Barnes, K. Miettunen, X. Li, A. Y. Anderson, T. Bessho, M. Gratzel, B. C. O'Regan, *Adv. Mater.* **2013**, *25*, 1881.
[7] S. M. Feldt, E. A. Gibson, E. Gabrielsson, L. Sun, G. Boschloo, A. Hagfeldt, *J. Am. Chem. Soc.* **2010**, *132*, 16714.
[8] A. Yella, H.-W. Lee, H. N. Tsao, C. Yi, A. K. Chandiran, M. K. Nazeeruddin, E. W.-G. Diau, C.-Y. Yeh, S. M. Zakeeruddin, M. Grätzel, *Science* **2011**, *334*, 629.
[9] B. C. O'Regan, J. R. Durrant, *Acc. Chem. Res.* **2009**, *42*, 1799.
[10] L. M. Peter, *Phys. Chem. Chem. Phys.* **2007**, *9*, 2630.
[11] A. K. Chandiran, N. Tetreault, R. Humphry-Baker, F. Kessler, E. Baranoff, C. Yi, M. K. Nazeeruddin, M. Grätzel, *Nano Lett.* **2012**, *12*, 3941.
[12] T. C. Li, M. S. Góes, F. Fabregat-Santiago, J. Bisquert, P. R. Bueno, C. Prasittichai, J. T. Hupp, T. J. Marks, *J. Phys. Chem. C* **2009**, *113*, 18385.
[13] T. W. Hamann, O. K. Farha, J. T. Hupp, *J. Phys. Chem. C* **2008**, *112*, 19756.
[14] C. Prasittichai, J. T. Hupp, *J. Phys. Chem. Lett.* **2010**, *1*, 1611.
[15] H.-J. Son, X. Wang, C. Prasittichai, N. C. Jeong, T. Aaltonen, R. G. Gordon, J. T. Hupp, *J. Am. Chem. Soc.* **2012**, *134*, 9537.
[16] S. M. Feldt, U. B. Cappel, E. M. J. Johansson, G. Boschloo, A. Hagfeldt, *J. Phys. Chem. C* **2010**, *114*, 10551.
[17] M. J. Katz, M. J. D. Vermeer, O. K. Farha, M. J. Pellin, J. T. Hupp, *Langmuir* **2012**, *29*, 806.
[18] M. J. DeVries, M. J. Pellin, J. T. Hupp, *Langmuir* **2010**, *26*, 9082.
[19] M. Shanmugam, M. F. Baroughi, D. Galipeau, *Thin Solid Films* **2010**, *518*, 2678.
[20] L. J. Antila, M. J. Heikkilä, V. Aumanen, M. Kemell, P. Myllyperkiö, M. Leskelä, J. E. I. Korppi-Tommola, *J. Phys. Chem. Lett.* **2009**, *1*, 536.
[21] K. E. Roelofs, T. P. Brennan, J. C. Dominguez, C. D. Bailie, G. Y. Margulis, E. T. Hoke, M. D. McGehee, S. F. Bent, *J. Phys. Chem. C* **2013**, *117*, 5584.
[22] B. C. O'Regan, S. Scully, A. C. Mayer, E. Palomares, J. Durrant, *J. Phys. Chem. B* **2005**, *109*, 4616.
[23] K. Hanson, M. D. Losego, B. Kalanyan, D. L. Ashford, G. N. Parsons, T. J. Meyer, *Chem. Mater.* **2012**, *25*, 3.
[24] J. W. Elam, D. Routkevitch, P. P. Mardilovich, S. M. George, *Chem. Mater.* **2003**, *15*, 3507.
[25] M. Leskelä, M. Ritala, *Thin Solid Films* **2002**, *409*, 138.
[26] S. M. George, *Chem. Rev.* **2009**, *110*, 111.
[27] Y. Xu, M. Schoonen, *Am. Mineralogist* **2000**, *85*, 543.
[28] H. N. Tsao, C. Yi, T. Moehl, J.-H. Yum, S. M. Zakeeruddin, M. K. Nazeeruddin, M. Grätzel, *ChemSusChem* **2011**, *4*, 591.
[29] A. K. Chandiran, P. Comte, R. Humphry-Baker, F. Kessler, C. Yi, M. K. Nazeeruddin, M. Grätzel, *Adv. Funct. Mater.* **2013**, *23*, 2775.
[30] C. L. Dezelah, J. Niinistö, K. Arstila, L. Niinistö, C. H. Winter, *Chem. Mater.* **2005**, *18*, 471.
[31] D. M. Hausmann, E. Kim, J. Becker, R. G. Gordon, *Chem. Mater.* **2002**, *14*, 4350.
[32] K. Kukli, M. Ritala, M. Leskelä, *J. Electrochem. Soc.* **1995**, *142*, 1670.
[33] T. Blanquart, J. Niinistö, M. Heikkilä, T. Sajavaara, K. Kukli, E. Puukilainen, C. Xu, W. Hunks, M. Ritala, M. Leskelä, *Chem. Mater.* **2012**, *24*, 975.
[34] A. K. Chandiran, A. Yella, M. Stefik, L.-P. Heiniger, P. Comte, M. K. Nazeeruddin, M. Grätzel, *ACS Appl. Mater. Interfaces* **2013**, *5*, 3487.
[35] A. R. Burke, C. R. Brown, W. C. Bowling, J. E. Glaub, D. Kapsch, C. M. Love, R. B. Whitaker, W. E. Moddeman, *Surf. Interface Anal.* **1988**, *11*, 353.
[36] G. Schön, *J. Electron Spectrosc. Relat. Phenom.* **1973**, *2*, 75.
[37] R. Jerome, P. Teyssie, J. J. Pireaux, J. J. Verbist, *Appl. Surf. Sci.* **1986**, *27*, 93.
[38] M. A. B. Gomes, L. O. de S. Bulhões, S. C. de Castro, A. J. Damião, *J. Electrochem. Soc.* **1990**, *137*, 3067.
[39] E. Atanassova, T. Dimitrova, J. Koprinarova, *Appl. Surf. Sci.* **1995**, *84*, 193.
[40] H. Tang, K. Prasad, R. Sanjines, P. E. Schmid, F. Levy, *J. Appl. Phys.* **1994**, *75*, 2042.
[41] S. Ito, T. N. Murakami, P. Comte, P. Liska, C. Grätzel, M. K. Nazeeruddin, M. Grätzel, *Thin Solid Films* **2008**, *516*, 4613.
[42] N. W. Duffy, L. M. Peter, R. M. G. Rajapakse, K. G. U. Wijayantha, *Electrochem. Commun.* **2000**, *2*, 658.
[43] H. A. Huy, B. Aradi, T. Frauenheim, P. Deak, *J. Appl. Phys.* **2012**, *112*, 16103.
[44] J. Osorio-Guillén, S. Lany, A. Zunger, *Phys. Rev. Lett.* **2008**, *100*, 36601.
[45] S. X. Zhang, D. C. Kundaliya, W. Yu, S. Dhar, S. Y. Young, L. G. Salamanca-Riba, S. B. Ogale, R. D. Vispute, T. Venkatesan, *J. Appl. Phys.* **2007**, *102*, 13701.

[46] A. M. Ruiz, G. Dezanneau, J. Arbiol, A. Cornet, J. R. Morante, *Chem. Mater.* **2004**, *16*, 862.
[47] A. K. Chandiran, F. Sauvage, M. Casas-Cabanas, P. Comte, S. M. Zakeeruddin, M. Graetzel, *J. Phys. Chem. C* **2010**, *114*, 15849.
[48] A. K. Chandiran, F. Sauvage, L. Etgar, M. Graetzel, *J. Phys. Chem. C* **2011**, *115*, 9232.
[49] J. Bisquert, *J. Phys. Chem. B* **2001**, *106*, 325.
[50] S. E. Koops, B. C. O'Regan, P. R. F. Barnes, J. R. Durrant, *J. Am. Chem. Soc.* **2009**, *131*, 4808.